Contrib Mineral Petrol (2010) 160:67–81
DOI 10.1007/s00410-009-0466-6

ORIGINAL PAPER

Tectonic implications of garnet-bearing mantle xenoliths exhumed by Quaternary magmatism in the Hangay dome, central Mongolia

Nigel Harris · Alison Hunt · Ian Parkinson · Andrew Tindle · Magisuren Yondon · Samantha Hammond

Received: 25 July 2009 / Accepted: 13 November 2009 / Published online: 1 December 2009

Abstract Garnet-bearing mantle xenoliths have been recovered from Quaternary alkali basalts, both within and peripheral to the Hangay dome of central Mongolia. Microfabric analysis and thermobaromery, combining empirical thermobarometers and the self-consistent dataset of THERMOCALC, indicate that garnet websterites from the Shavaryn-Tsaram volcanic centre at the dome core were formed in the spinel-lherzolite upper mantle at pressures of 17–18 kbars and temperatures of 1,070–1,090°C, whereas garnet lherzolites were derived from greater depths (18–20 kbars). Garnet lherzolites from the Baga Togo Uul vents near the dome edge were formed at 18–22 kbars under significantly cooler conditions (960–1,000°C). These xenoliths reveal reaction coronas of (1) orthopyroxene, clinopyroxene, plagioclase and spinel mantling garnets; (2) spongy rims of olivine replacing orthopyroxene and (3) low-Na, low-Al clinopyroxene replacing primary clinopyroxene. Trace-element abundances indicate that clinopyroxene from these coronas is in chemical equilibrium with the host magma. The thermobarometric and textural data suggest that lherzolite xenoliths from both sites were derived from depths of 60–70 km and entrained in magma at 1,200–1,300°C. The average rate of ascent, as determined by olivine zoning, lies in the range 0.2–0.3 m s^{-1}. The contrast in thermal profiles of the upper mantle between the two sites is consistent with a mantle plume beneath the Hangay dome with elevated thermal conditions beneath the core of the dome being comparable to estimates of the Pleistocene geotherm beneath the Baikal rift.

Keywords Intra-plate volcanism · Xenoliths · Thermobarometry · Mongolian tectonics

Communicated by C. Ballhaus.

N. Harris (✉) · A. Hunt · I. Parkinson · A. Tindle · S. Hammond
Department of Earth and Environmental Sciences, The Open University, Milton Keynes MK7 6AA, UK
e-mail: n.b.w.harris@open.ac.uk

M. Yondon
School of Geology, Mongolian University of Science, and Technology (MUST), P.O. Box 49/418, Ulaanbaatar, Mongolia

Introduction

A significant proportion of the Earth's magma generation and seismic activity occurs well within the continents, distant from any plate margins, and the causes of such magmatism hold the key to understanding how the continental lithosphere behaves in plate interiors. Central Asia, where deformation and magmatism is distant from active plate margins, provides an ideal environment for studying intra-plate tectonics. Alkali basaltic vents and flows from central Mongolia range in age from about 30 million to about 8,000 years ago (Barry et al. 2003; Chuvashova et al. 2007); many of these are distributed within and around a topographic rise, known as the Hangay dome (Fig. 1). This mountainous region covers an area over 200,000 km^2 rising to elevations of 4,000 m. The dome forms a critical tectonic link between the Baikal rift to the north and the Altai transpressional domain, related to the India–Asia collision, to the south. It is underlain by a fragment of cratonic basement, comprising Precambrian gneisses and schists, encircled by Neoproterozoic to Paleozoic mobile belts (Badarch et al. 2002). These are collectively termed the Central Asian orogenic belt which bounds the southern margin of the Siberian craton (Windley et al. 2007).

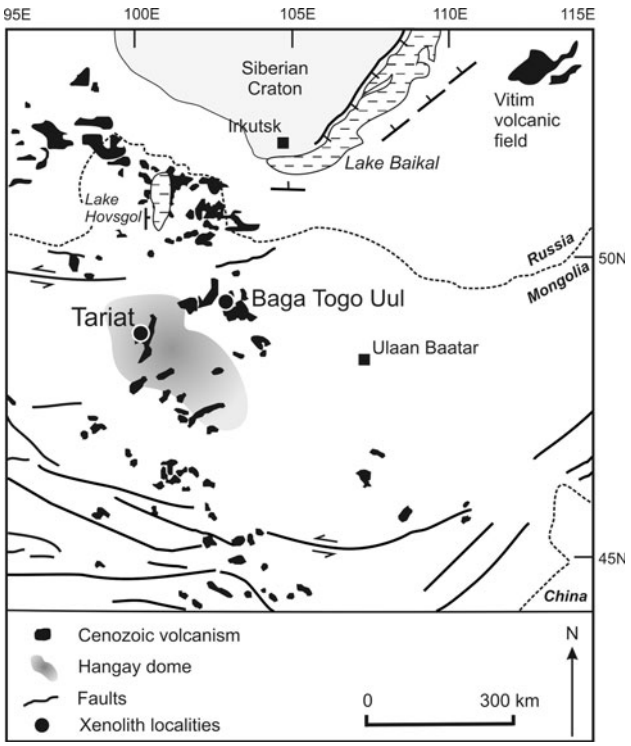

Fig. 1 Schematic map of central Mongolia and southern Siberia showing distribution of Cenozoic volcanics, regional faulting and the Hangay dome (shown for elevations >2,000 m); compiled from Badarch et al. (2002), Barry et al. (2003), Walker et al. (2008). Xenolith localities are at Tariat and at Baga Togo Uul

Although the dome is seismically quiescent, neotectonic studies indicate that it is a region of persistent tectonic activity dominated by left-lateral shear (Walker et al. 2008). The cause of the Hangay magmatism remains uncertain being variously ascribed to a mantle plume (Windley and Allen 1993) as has been proposed for magmatism associated with the Baikal rift to the north (Johnson et al. 2005), or to the removal of a deep lithospheric keel by convective circulation deep within the asthenosphere (Cunningham 2001), which could cause not only uplift and doming at the surface but also result in mantle melting at depth, as has been invoked for the recent volcanism on the Tibetan Plateau (Williams et al. 2004).

Flows and pyroclastics from several of the volcanic centres of the Hangay dome contain xenoliths of garnet granulites of crustal origin and garnet pyroxenites, garnet lherzolites and spinel lherzolites from the mantle lithosphere (Ionov et al. 1992; Barry et al. 2003). Precise pressure–temperature estimates on mantle xenoliths constrain minimum depths from which melts are formed and yield temperature-depth arrays for the lithosphere at the time of magma extrusion, critical for understanding the causes of magmatism. All published data from garnet-bearing mantle xenoliths in Mongolia (Kopylova et al. 1995; Stosch et al. 1995; Ionov et al. 1998; Ionov 2007) derive from the Tariat region of cones located in the central region of the Hangay dome (Fig. 1).

This paper presents robust thermobarometry from the mineral assemblages of garnet-bearing ultramafic xenoliths collected from both the central region of the dome (Tariat) and from the Baga Togo Uul volcano outlying the north-east margin of the dome. Garnet-bearing xenoliths are rare from the latter locality, but the results obtained from two such samples provide quantitative constraints on the thermal structure beneath the margin of the Hangay dome thus providing the first comparative xenolith study from two regions distributed across the dome (Fig. 1). Equilibrium assemblages have been identified by textural observation and by assessing intra-grain zoning by core-rim analyses using the electron microprobe, thus allowing endmember activities to be calculated and PT estimates obtained using a combination of empirical geothermometers and geobarometers and, where appropriate, the software package THERMOCALC (Holland and Powell 1998, 2003). The latter approach optimises the use of available equilibria for thermobarometry and propagates realistic uncertainties, incorporating consistent assumptions in the activity calculations. Results from xenoliths recovered from the dome margin have been compared with an empirical geotherm established from samples taken from the core of the dome, the two sites being separated by ca. 230 km, in order to constrain the dimensions of the thermal perturbation in the upper mantle. This study enhances our understanding of the thermal structure of the sub-continental lithospheric mantle and its contribution to intra-plate magmatism.

The Tariat xenoliths

A plethora of vents and cones are exposed in the Tariat region of central Mongolia, the youngest (Holocene), best-preserved and highest (2,965 m) being Khorgo Uul, dated by ^{14}C isotopes on organic material from interbedded sediments at ca. 8 ka (Chuvashova et al. 2007). The lavas range in composition from alkali basalts, trachybasalts to tephrite basanites (Barry et al. 2003; Hunt et al. 2008). Although crustal granulites and spinel lherzolite xenoliths are commonly found in flows throughout the Tariat region, garnet-bearing mantle xenoliths have only been recovered from the volcanic centres of Shavaryn-Tsaram and Zala (Ionov et al. 1998). Shavaryn-Tsaram, located 10 km south-east of Tariat, comprises basaltic tuffs and breccias entraining abundant xenoliths (Kopylova et al. 1995) that are distributed over an area of ca. 0.5 km^2. In addition to the pyroclastics, vesicular alkali basalt flows form the floor of the adjacent river valley (Press et al. 1986). The only chronological constraint from Shavaryn-Tsaram is a K–Ar

age from the lavas of ca. 1.2 Ma (Agafonov et al. 1975); this lies within the range (0.6–5.9 Ma) defined by Ar–Ar chronology in the Tariat area (Barry et al. 2003) and is coeval with Pleistocene flows (1.3 ± 0.1 Ma) that dominate the region (Schlupp 1996).

Xenoliths from the Shavaryn-Tsaram centre include granulites, lherzolites and pyroxenites; these are commonly up to 6 cm across, although rare mantle-derived bombs measuring 0.5 m across have also been recovered (Harris 2009). A pressure estimate of 14.0 ± 1.5 kbars has previously been obtained from a kelyphitic pyroxenite from Shavaryn-Tsaram (Stosch et al. 1995). More recently thermobarometric constraints on xenoliths from the Tariat region have been published in Ionov (2007), who obtained pressures from garnet lherzolites (using the empirical calibrations of Nickel and Green 1985) and temperatures for spinel lherzolites, derived from Ca concentrations in orthopyroxene (Brey and Köhler 1990) and two-pyroxene thermometry (Wells 1977), to infer a possible geotherm. Results from a single kelyphitic lherzolite xenolith (Z-68, from the Zala cone, located 6 km north of Shavaryn-Tsaram) yielded pressures of 1.96 GPa and temperatures of 1,088°C. Pressures for the spinel lherzolites were obtained by assuming a linear geotherm throughout the calculated temperature range. This approach is subject to under-estimation of temperatures due to subsolidus re-equilibration potentially resulting in underestimations of $\Delta T/\Delta P$ for the apparent geotherm. Previous studies of crustal and mantle xenoliths from the Tariat region (Stosch et al. 1995; Kopylova et al. 1995; Ionov 2002) constrain the Moho to depths of 13–15 kbars, suggesting crustal thicknesses of ca. 45 km at the time of volcanism.

The Baga Togo Uul xenoliths

In the Togo region of northern Mongolia, several Cenozoic volcanic centres (mostly of basaltic trachyandesite and tephrite basanite composition) intrude the Permo-Triassic Selenge belt (Badarch et al. 2002). In contrast to the Tariat vents, the volcanics from the Togo region are poorly studied and the only record of garnet-bearing xenoliths in the literature, prior to this study, is a passing reference by Sobolev and Nixon (1987) to the presence of garnet in mantle xenoliths. Uran Uul, the youngest and highest volcano in the cluster (ca. 1,700 m), is probably Holocene in age judging from its well-preserved steep-sided conical form. However, no xenoliths were found within lavas from this cone. Our work focuses on xenoliths from Baga Togo Uul, a volcano with three slightly eroded vents (Togo and two adjacent vents, Tulga and Javalach) that rise to altitudes of 1,600 m. We recovered several garnet-lherzolite xenoliths ranging in size from 5 to 20 mm, the best preserved being from the Tulga vent. The precise age of these eruptions is unknown but they certainly predate the bronze to early iron-age standing stones in the craters (3–4 ka). Their slightly eroded profiles (the vent walls have been breached by erosion in the smaller vents yet the overall conical form is preserved) suggest they pre-date the well-preserved cone of the Holocene volcano Khorgo Uul, and are of similar age (ca. 1 Ma) to Pleistocene cones from east and south of Tariat (Schlupp 1996). Until radiometric dating is undertaken, we infer that the Baga Togo Uul volcano is Quaternary, and most probably Pleistocene, in age.

Methodology

Mineral compositions (major elements) were analysed using a Cameca SX100 electron microprobe operating in wavelength-dispersive mode at an operating voltage of 20 kV and probe current of 20 nA (measured on a Faraday cage) with a beam 10 μm in diameter, reduced to 5 μm for mineral traverses. Count times varied from 20 to 60 s per element, and data were corrected using a PAP correction procedure (Pouchou and Pichoir 1985). The following standards and X-ray lines were used: jadeite (Na Kα), forsterite (Mg Kα), K-feldspar (Al Kα, Si Kα, K Kα), rutile (Ti Kα), bustamite (Mn Kα, Ca Kα), hematite (Fe Kα).

Trace-element abundances in garnet and clinopyroxene grains were determined at the Open University by an Agilent 7500s ICP-MS coupled with a New Wave 213 Nd:YAG UV (213 nm) laser system, firing at 10 Hz. Samples were ablated in a pure He atmosphere, and the analyte carried in He and mixed with argon via a ''Y'' connector before entering the plasma. The use of He gives a 2–3-fold increase in sensitivity, and significantly reduces background intensity (Günther and Heinrich 1999). Data were acquired across the mass range from ^{7}Li to ^{238}U, using a 40 μm (Tulga samples) and 80 μm (Tariat samples) spot size. The total time for each analysis was 220 s; during the first 100 s, the gas blank is measured whilst the laser beam is blocked by a shutter. The sample is then ablated for 60 s, and the transient signals from the analyte are acquired for a further 60 s. Analyses were separated by a 210 s wash out period. Data were reduced using the GLITTER software (Griffin et al. 2008). The NIST 612 glass standard provided an external calibration. In addition, we analysed the K-23 garnet standard (courtesy of T. Zack); our analyses of REE from this study replicate those produced in six other laboratories to within one standard deviation of the mean. Detection limits lie between 1 and 18 ppb.

Petrography and major-element mineral chemistry

Shavaryn-Tsaram volcanic centre (Tariat region)

Garnet-bearing ultramafic xenoliths recovered from the Shavaryn-Tsaram volcanic centre (06-07, 18-07, Table 1) comprise granoblastic websterite assemblages (0.5–4 mm grainsize) of clinopyroxene, orthopyroxene and garnet (72–74% pyrope, 13–17% almandine, 11–12% grossular, 6–8% spessartine). Orthopyroxenes are relatively small and unzoned whereas some larger garnet grains show a slight decrease in Mg number towards the rim (Mg# from 84 to 81) and clinopyroxene grains show a small decrease in Mg# from 91 to 89 (Table 2). Small prismatic grains of spinel have been identified within the kelyphitic rims with low chrome contents ($Cr_2O_3 < 0.6\%$). Polygonal grain boundaries suggest textural equilibrium with the exception of the kelyphitic rims mantling the garnets (Fig. 2a).

Tulga and Javalach vents (Togo region)

Garnet lherzolite xenoliths from the Tulga vent (03-08, 06-08, Table 1) consist of garnet (72–74% pyrope, 13–14% almandine, 12–13% grossular, 7% spessartine), Cr-bearing clinopyroxene ($Cr_2O_3 \approx 1\%$), orthopyroxene and olivine; grain size is 0.5–1 mm. Larger olivine grains are zoned with Mg# = 89 in core with relatively Mg-poor rims, Mg# = 82 (Fig. 3). Forsterite-poor rims are confined to the outer 70 μm of the grains (Fig. 3). Small disseminated grains of Cr-rich spinel ($Cr_2O_3 \approx 17\%$) are distributed along olivine grain boundaries. Pyroxenes are unzoned as is garnet except where it is associated with corona textures (see below). Garnet was not observed in contact with spinel. Mineral compositions are presented in Table 3.

A range of spectacular reaction textures have been developed in xenoliths collected from the Tulga and Javalach vents of Baga Togo Uul:

1. Garnet grains are rimmed by a corona of plagioclase (labradorite), clino- and orthopyroxene and Cr-rich spinel (Fig. 2b, c). Clino- and orthopyroxenes in the corona assemblages are depleted in the Mg-rich endmember relative to core compositions from the primary assemblage. The outer narrow rim (<20 μm wide) of garnet in contact with the corona is slightly depleted in Mg and Ca (Table 3).
2. Orthopyroxene grains on the margins of the xenolith (i.e. in contact with crystallised melt) are rimmed by spongy olivine with vermicular intergrowths (Fig. 2d). The composition of the spongy mantle is depleted in forsterite (Mg# = 78) relative to primary olivine (Table 3).
3. In some xenoliths from Javalach, clinopyroxene grains are rimmed by spongy vermicular aggregates of clinopyroxene (Fig. 2e) that are depleted in Na and Al relative to the core of the grain (Table 3). Major-elements in the unreacted core do not vary in composition.

Trace-element mineral chemistry

Garnet and clinopyroxene spot analyses were obtained by ICP-MS for grains from 06-07 (Tariat region, Fig. 2a) and 03-08 (Baga Togo Uul region, Fig. 2b, e). Results are presented in Table 4.

Garnet

Trace-element analyses from core and rim of garnets from both the Tariat region and the Tulga vent of Baga Togo Uul indicate no significant zoning across the grain except for HREE which show slight enrichment towards the core (Fig. 4a, b), a feature that is more pronounced in the Tulga sample. Garnet is depleted in all elements relative to the bulk-rock (bulk rock data from Barry et al. 2003) except for Y and HREE. Chondrite-normalised REE plots confirm strong enrichment in HREE, relative to LREE for both garnets (Fig. 4c, d).

Table 1 Xenolith samples and localities

Sample number	Rock-type	Longitude (E)	Latitude (N)	Altitude (m)
Tariat region				
06-07 (Shavaryn-Tsaram centre)	Garnet websterite + spinel	99° 59.56′	48° 02.38′	2,376
18-07 (Shavaryn-Tsaram centre)	Garnet websterite	99° 59.56′	48° 02.38′	2,376
Baga Togo Uul				
03-08 (Tulga vent)	Garnet lherzolite + spinel, plagioclase	102° 46.17′	48° 56.14′	1,473
06-08 (Tulga vent)	Garnet lherzolite + spinel	102° 46.17′	48° 56.14′	1,473
13-08 (Javalach vent)	Spinel lherzolite	102° 44.38′	48° 55.73′	1,491

Table 2 Representative mineral compositions from mantle xenoliths (Shavaryn-Tsaram, Tariat region)

wt%	Garnet					Orthopyroxene				Clinopyroxene				Spinel
	06-07 Core	06-07 Rim	18-07 Core	18-07 Rim		06-07 Core	06-07 Rim	18-07 Core		06-07 Core	06-07 Rim	18-07 Core		06-07 Reaction rim
SiO_2	42.26	42.46	41.94	41.82		53.82	54.11	54.00		51.63	51.54	51.56		0.13
TiO_2	0.12	0.20	0.19	0.33		0.20	0.24	0.21		0.57	0.56	0.59		0.12
Al_2O_3	23.23	23.59	23.29	23.03		6.01	5.50	5.54		7.42	7.85	7.14		65.12
Cr_2O_3	0.16	0.18	0.37	0.32		0.19	0.21	0.24		0.63	0.12	0.55		0.56
Fe_2O_3[a]	1.19	1.31	0.62	0.65		0.23	0.25	0.00		0.83	0.44	0.44		1.95
FeO	6.87	6.58	7.16	8.31		6.60	6.53	6.85		2.78	3.51	3.33		8.46
MnO	0.34	0.35	0.33	0.39		0.15	0.14	0.15		0.08	0.11	0.09		0.16
MgO	20.90	21.17	20.64	20.01		31.11	31.26	31.07		15.46	15.43	15.63		21.80
CaO	4.71	4.83	4.68	4.14		1.14	1.15	1.10		18.04	17.24	17.47		0.03
Na_2O	0.03	0.02	0.01	0.11		0.19	0.23	0.19		1.88	1.89	1.83		0.01
K_2O	0.00	0.00	0.00	0.04		0.00	0.00	0.00		0.00	0.05	0.01		0.00
Total	99.81	100.69	99.23	99.15		99.64	99.62	99.35		99.32	98.74	98.64		98.34
(O)	12	12	12	12		6	6	6		6	6	6		3
Si	2.990	2.976	2.986	2.993		1.872	1.882	1.884		1.871	1.876	1.881		0.003
Ti	0.006	0.010	0.010	0.017		0.005	0.006	0.005		0.015	0.015	0.016		0.002
Al	1.937	1.949	1.954	1.943		0.246	0.225	0.227		0.317	0.336	0.307		1.940
Cr	0.008	0.009	0.020	0.018		0.005	0.005	0.006		0.018	0.003	0.015		0.011
Fe^{+3}	0.063	0.069	0.033	0.035		0.006	0.006	0.000		0.022	0.012	0.012		0.037
Fe^{+2}	0.406	0.386	0.426	0.497		0.192	0.190	0.199		0.084	0.107	0.101		0.178
Mn	0.020	0.020	0.019	0.023		0.004	0.004	0.004		0.002	0.003	0.002		0.003
Mg	2.204	2.211	2.190	2.134		1.612	1.620	1.616		0.835	0.837	0.849		0.821
Ca	0.357	0.362	0.357	0.317		0.042	0.042	0.041		0.700	0.672	0.682		0.000
Na	0.004	0.002	0.001	0.015		0.012	0.015	0.012		0.132	0.133	0.129		0.000
K	0.000	0.000	0.000	0.003		0.000	0.000	0.000		0.000	0.002	0.000		0.000
Mg#	84.44	85.14	83.72	81.11		89.36	89.50	89.04		90.86	88.67	89.37		82.18
Activities[b]														
py	0.41	0.42	0.41	0.37	en	0.65	0.65	0.65	di	0.51	0.46	0.49	sp	0.79
gr	0.009	0.010	0.010	0.006	fs	0.010	0.010	0.011	heds	0.072	0.085	0.085	herc	0.190
alm	0.0021	0.0018	0.0025	0.0040	mgts	0.099	0.089	0.093	cats	0.230	0.250	0.230	mt	0.0019

[a] Calculated from stoichiometry

[b] As determined by Ax for THERMOCALC; See Holland and Powell (2003) for endmember abbreviations

Clinopyroxene

Core and rim analyses for large clinopyroxene grains show little variation in either sample, all pyroxenes being depleted in large-ion lithophile (LIL) elements Rb, Ba, Th, U, and the high-field-strength (HFS) elements Nb and Ta (Fig. 4a, b). REE profiles are slightly enriched in middle REE (Fig. 4c, d). Clinopyroxene from the spongy corona surrounding larger clinopyroxene grains in the Tulga sample (Fig. 2e) is enriched in all trace elements relative to the core and rim analyses from the unreacted primary grain (Fig. 4b) but is particularly enriched in LILE. The REE profile of the corona clinopyroxene is similar in form to analyses of the primary clinopyroxene.

Thermobarometry

Pressure–temperature fields have been calculated for six garnet-bearing mantle xenoliths (four from data presented here, two from data presented by Ionov et al. 1998) using empirical two-pyroxene thermometry (Brey and Köhler 1990) and enstatite-in-clinopyroxene thermometry (Nimis and Taylor 2000) and barometry using two independent calibrations; Al in orthopyroxene (Brey and Köhler 1990) and Cr in clinopyroxene (Nimis and Taylor 2000). Results are presented in Table 5. Endmember activities for each composition were calculated using the programme AX (Holland and Powell 2003), and equilibria assessed using THERMOCALC (Holland and Powell 1998). To obtain

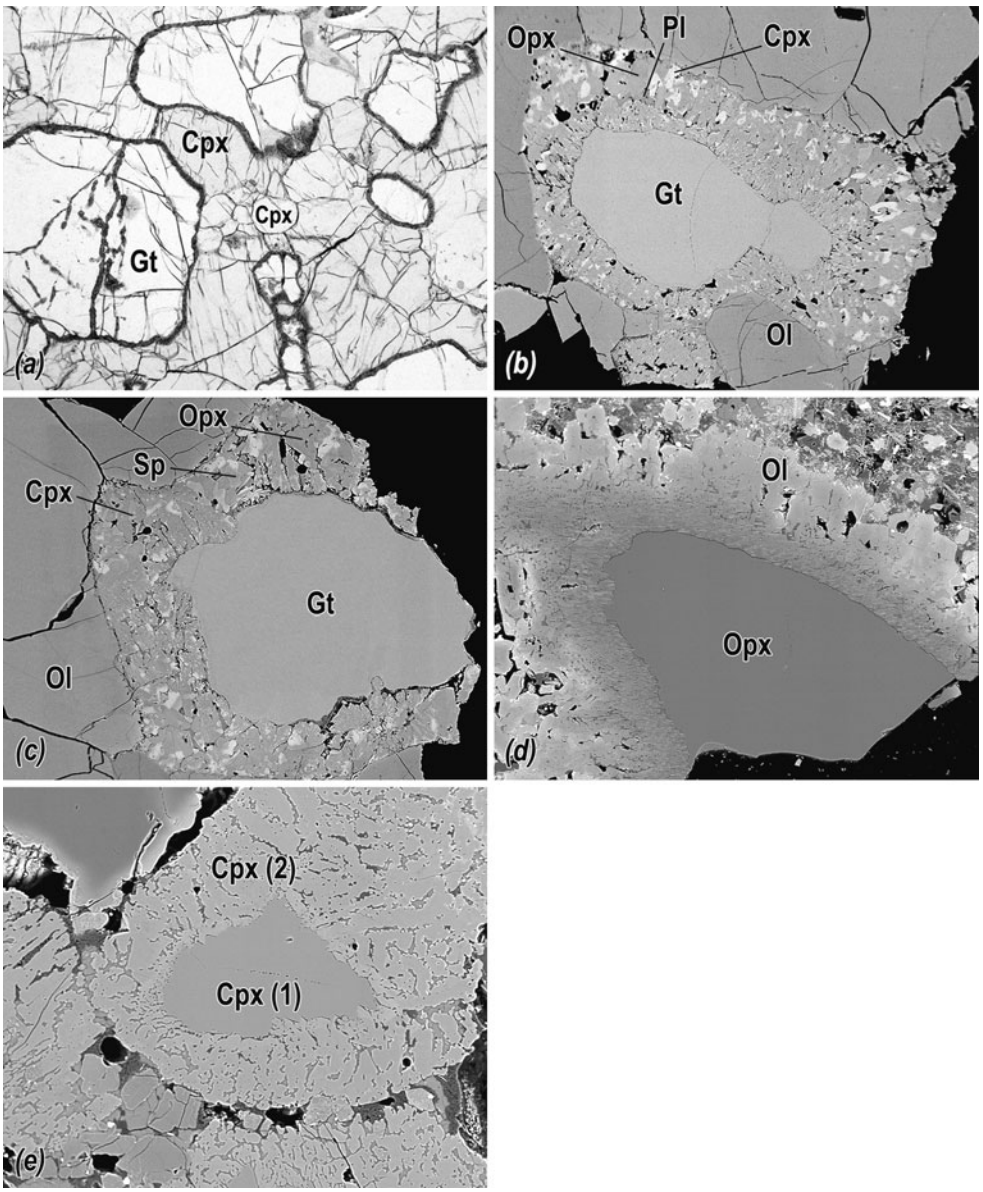

Fig. 2 Micro-images of mineral assemblages from garnet-bearing mantle xenoliths. **a** Garnet with kelyphitic rims in websterite; sample 06-07, Shavaryn-Tsaram volcanic centre, Tariat region (width of image = 10 mm, plane polarised light). **b** Garnet corona of orthopyroxene, clinopyroxene and plagioclase in lherzolite; sample 03-08, Tulga vent, Baga Togo Uul (width of BSE image = 2 mm). **c** Corona of orthopyroxene, clinopyroxene and spinel mantling garnet in lherzolite; sample 06-08, Tulga vent, Baga Togo Uul (width of BSE image = 1 mm). **d** Orthopyroxene mantled by olivine adjacent to melt in lherzolite; sample 03-08, Tulga vent, Baga Togo Uul (width of BSE image = 1.5 mm). **e** Clinopyroxene (Cpx(1)) mantled by spongy, low-Na, low-Al clinopyroxene (Cpx(2)) in spinel lherzolite; sample 13-08, Javalach vent, Baga Togo Uul (width of BSE image = 0.5 mm). *Gt* garnet, *Opx* orthopyroxene, *Cpx* clinopyroxene, *Ol* olivine, *Pl* plagioclase, *Sp* spinel

initial conditions of formation, core compositions of large grains from the primary assemblage (i.e. not within coronas or associated with reaction rims) were used for each phase.

Shavaryn-Tsaram (Tariat region)

The websterite samples (06-07, 18-07) formed within the spinel-lherzolite mantle at pressures of 17–18 kbars and temperatures of ~1,090°C. We also ran mineral compositions from two garnet-lherzolite xenoliths from Shavaryn-Tsaram (ST-1) and from Zala (Z68) published by Ionov et al. (1998) using the same empirical thermometers and barometers as for the websterite samples. The purpose of re-running these compositions for this study was to assess whether the difference in methodology between our work and previous studies generated systematic differences in the PT estimates. Results indicate that the Tariat garnet-lherzolite xenoliths yield conditions of $P = 18$–20 kbars,

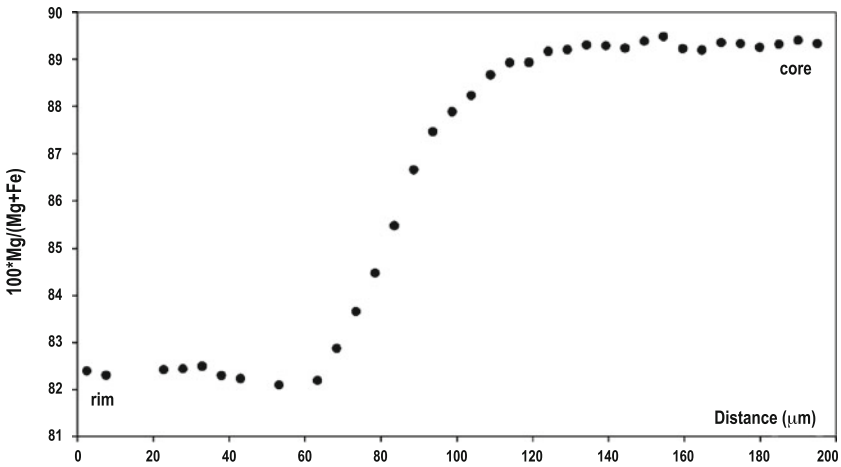

Fig. 3 Zoning in Mg# (100*MgO/(MgO + FeO) in mole %) across 0.4 mm grain from rim (distance = 0) to core (distance = 200 μm). Sample from Tulga garnet lherzolite (03-08). Beam size = 5 μm

T = 1,070–1,090°C (Fig. 5) which lie just above the steep linear geotherm (G_o, Fig. 5) derived by Ionov (2007) on the basis of 35 xenoliths of garnet and spinel-bearing peridotites. Results for the garnet websterites also fall slightly above G_o. Given realistic minimum uncertainties on the empirical thermobarometers (±30°C for temperatures, ±2 kbar for pressures, see Nimis and Taylor 2000) the calculated field lies within error of the empirical geotherm G_o confirming that although we employ a different methodology to previous studies our results for the Tariat lherzolites do not differ significantly. In any event these data confirm an unusually steep geotherm (high dT/dP) beneath the core of the Hangay dome at the time of magmatism, estimated at ca. 80°C/kbar within the crust (Ionov et al. 1998) and our results suggest this may be a slight underestimate. THERMOCALC calculations for activities on relevant endmembers from all Tariat xenoliths failed to obtain barometric estimates due to lack of equilibria with marked changes in molar volumes, and obtained temperature estimates with too high an uncertainty (>200°C) to be useful.

Tulga (Togo region)

Using the same array of thermobarometers as applied to samples from the Tariat centres, we conclude that the Tulga xenolith 03-08 equilibrated at P = 18–22 kbars, T = 960–1,000°C; a second garnet lherzolite (06-08) lies within this field (Table 5). This suggests a significantly shallower geotherm (low dT/dP) prevailed beneath the Togo region compared with the Tariat area (Fig. 5).

The corona developed around the garnet grains provides appropriate assemblages to determine the conditions under which the corona developed. The principal decompression reactions represented by the corona are:

$$\text{Garnet} + \text{Olivine} = \text{Orthopyroxene} + \text{Spinel} \quad (1)$$

$$\text{Garnet} + \text{Clinopyroxene} = \text{Orthopyroxene} + \text{Olivine} + \text{Plagioclase} \quad (2)$$

Given the potassic content in plagioclase (1 wt%), the basaltic melt could be an additional reactant in reaction (2). Reaction (1) defines the boundary between spinel and garnet lherzolites. Using the same empirical geothermometers as described above for the core compositions of phases, the corona assemblages surrounding garnets, combined with rim compositions for garnets adjacent to the coronas, yield conditions of P = 12.5–15.0 kbars, T = 1,190–1,225°C for garnet lherzolite sample 03-08. The presence of plagioclase in the corona allows these results to be compared with outputs from THERMOCALC thermobarometry (Holland and Powell 1998, 2003). This yielded an average-pressure path that passes through the field defined by empirical thermobarometry based on pyroxene and garnet compositions (Fig. 5). All equilibria identified by THERMOCALC have a shallow slope, making them imprecise for thermometry, but the two reactions yielding the steepest slope (3Diopside + 3mgts = 2Pyrope + Grossular; Enstatite + mgts = Pyrope, where mgts is the Mg-tschermakite orthopyroxene endmember) intersect the average-pressure path at 13.1 ± 0.9 kbars and 1,200 ± 180°C which we interpret as representing the conditions during which the corona microstructures developed. The corona developed around garnet in lherzolite 06-08 indicates higher pressures (17–20 kbars) at somewhat higher temperatures (~1,300°C). The average temperature derived from THERMOCALC for this sample is estimated at 1,270 ± 140°C, but the absence of plagioclase in the corona prevents a precise pressure being calculated.

Discussion

Xenolith entrainment and transport

The combined thermobarometry from the Tulga xenoliths suggests decompression through 4–5 kbars (implying a vertical transport distance of ca. 25 km between

Table 3 Representative mineral compositions from mantle xenoliths (Tulga and Javalach vents, Baga Togo Uul)

wt%	Garnet				Orthopyroxene				Clinopyroxene							
	03-08 Core	03-08 Rim	06-08 Core	06-08 Rim	03-08 Core	03-08 Garnet corona	06-08 Core	06-08 Garnet corona	03-08 Core	03-08 Garnet corona	06-08 Core	06-08 Garnet corona	03-08 Core	03-08 Cpx corona	13-08 Core	13-08 Cpx corona
SiO_2	41.57	42.36	42.13	41.86	53.80	49.50	54.40	50.40	51.83	49.26	51.98	50.78	52.07	50.92	51.94	52.63
TiO_2	0.15	0.16	0.17	0.14	0.16	0.13	0.17	0.15	0.69	0.51	0.66	0.16	0.65	0.79	0.67	0.73
Al_2O_3	22.86	22.53	22.89	22.87	4.22	11.31	4.19	10.74	6.38	9.57	6.41	8.12	6.53	4.12	6.82	2.73
Cr_2O_3	1.02	1.05	1.05	1.03	0.46	0.70	0.48	0.56	1.05	0.58	1.08	0.45	1.07	1.33	1.18	1.44
Fe_2O_3[a]	1.74	1.80	1.31	1.38	1.43	0.00	1.39	0.00	1.24	0.77	0.33	0.39	0.39	0.76	0.09	0.00
FeO	6.37	6.24	6.73	6.75	5.15	8.19	5.24	8.41	1.97	4.20	2.77	5.42	2.70	2.39	3.40	3.42
MnO	0.35	0.33	0.35	0.35	0.12	0.38	0.13	0.42	0.09	0.32	0.06	0.43	0.08	0.09	0.09	0.06
MgO	20.62	19.99	20.84	20.65	32.52	26.90	32.71	27.01	14.98	15.69	14.92	18.18	14.75	15.83	15.58	16.73
CaO	4.86	4.67	4.85	4.82	0.72	1.79	0.69	2.09	18.95	16.59	18.37	14.70	18.74	21.78	17.21	20.50
Na_2O	0.03	0.55	0.02	0.02	0.13	0.08	0.14	0.11	2.06	1.21	2.11	0.80	2.10	0.64	2.02	0.68
K_2O	0.00	0.02	0.00	0.00	0.00	0.00	0.00	0.02	0.00	0.00	0.00	0.02	0.01	0.01	0.01	0.03
Total	99.57	99.70	100.34	99.87	98.71	98.97	99.54	99.91	99.24	98.71	98.69	99.45	99.08	98.79	98.99	98.94
(O)	12	12	6	6	6	6	6	6	6	6	6	6	6	6	6	6
Si	2.959	3.009	2.975	2.971	1.885	1.754	1.889	1.771	1.884	1.803	1.898	1.839	1.895	1.881	1.888	1.932
Ti	0.008	0.008	0.009	0.007	0.004	0.003	0.004	0.003	0.018	0.014	0.018	0.004	0.017	0.021	0.018	0.020
Al	1.918	1.886	1.905	1.913	0.174	0.472	0.171	0.445	0.273	0.413	0.275	0.346	0.280	0.179	0.292	0.118
Cr	0.057	0.058	0.058	0.057	0.012	0.019	0.013	0.015	0.030	0.016	0.031	0.012	0.030	0.038	0.033	0.041
Fe^{+3}	0.093	0.096	0.069	0.073	0.037	0.000	0.036	0.000	0.034	0.021	0.009	0.010	0.010	0.021	0.002	0.000
Fe^{+2}	0.379	0.370	0.397	0.401	0.150	0.242	0.152	0.247	0.060	0.128	0.084	0.164	0.082	0.073	0.103	0.105
Mn	0.021	0.019	0.020	0.021	0.003	0.011	0.003	0.012	0.002	0.009	0.001	0.013	0.002	0.002	0.002	0.001
Mg	2.187	2.116	2.193	2.184	1.698	1.420	1.693	1.415	0.811	0.855	0.812	0.981	0.800	0.871	0.844	0.915
Ca	0.370	0.355	0.367	0.366	0.027	0.067	0.025	0.078	0.738	0.650	0.718	0.570	0.730	0.862	0.670	0.806
Na	0.004	0.075	0.002	0.002	0.008	0.005	0.009	0.007	0.145	0.085	0.149	0.056	0.148	0.045	0.142	0.048
K	0.000	0.001	0.000	0.000	0.000	0.000	0.000	0.000	0.000	0.000	0.000	0.000	0.000	0.000	0.000	0.001
Mg#	85.2	85.1	84.7	84.5	91.9	85.4	91.8	85.1	93.1	87.0	90.6	85.7	90.7	92.3	89.1	89.7
Activities[b]																
py	0.40	0.37	0.39	0.39	en	0.72	0.50	0.71	0.49	di	0.57	0.41	0.54	0.37	0.55	0.71	0.49	0.66
gr	0.011	0.008	0.009	0.009	fs	0.006	0.016	0.006	0.016	heds	0.060	0.125	0.078	0.107	0.079	0.083	0.091	0.114
alm	0.0017	0.0015	0.0019	0.0020	mgts	0.051	0.170	0.053	0.160	cats	0.220	0.370	0.220	0.210	0.230	0.099	0.240	0.085

Table 3 continued

wt%	Olivine						Spinel				Plagioclase
	03-08 Core	03-08 Rim	03-08 Garnet corona	06-08 Core	06-08 Rim		03-08 Core	03-08 Garnet corona	06-08 Garnet corona		03-08 Garnet corona
SiO_2	40.40	38.68	38.27	40.27	39.78		0.06	0.05	0.06		57.44
TiO_2	0.00	0.07	0.05	0.01	0.00		0.33	0.50	0.06		0.27
Al_2O_3	0.01	0.03	0.06	0.01	0.00		49.00	63.68	63.81		21.81
Cr_2O_3	0.01	0.04	0.05	0.00	0.00		16.60	3.92	3.64		0.01
Fe_2O_3[a]	0.00	0.00	0.00	0.00	0.00		2.42	0.40	0.61		2.09
FeO	10.70	17.29	20.56	10.26	14.31		10.89	10.36	10.14		0.00
MnO	0.13	0.24	0.33	0.13	0.22		0.13	0.23	0.23		0.11
MgO	48.18	42.41	39.96	48.50	45.25		18.59	20.45	20.63		2.13
CaO	0.06	0.27	0.19	0.06	0.18		0.00	0.02	0.02		9.46
Na_2O	0.01	0.02	0.03	0.00	0.00		0.01	0.01	0.01		5.03
K_2O	0.00	0.00	0.00	0.00	0.00		0.00	0.00	0.00		1.00
Total	99.50	99.04	99.49	99.24	99.74		98.03	99.62	99.21		99.35
(O)	4	4	4	4	4		3	3	3		8
Si	0.997	0.990	0.993	0.994	0.997		0.001	0.001	0.001		2.633
Ti	0.000	0.001	0.002	0.000	0.000		0.006	0.000	0.001		0.009
Al	0.000	0.001	0.001	0.000	0.000		1.575	1.909	1.910		1.178
Cr	0.000	0.001	0.001	0.000	0.000		0.358	0.078	0.073		0.000
Fe^{+3}	0.000	0.000	0.000	0.000	0.000		0.049	0.007	0.011		0.072
Fe^{+2}	0.221	0.370	0.446	0.212	0.300		0.248	0.220	0.215		0.000
Mn	0.003	0.005	0.007	0.003	0.005		0.003	0.004	0.004		0.004
Mg	1.772	1.619	1.545	1.785	1.690		0.755	0.775	0.780		0.145
Ca	0.001	0.007	0.005	0.001	0.005		0.000	0.000	0.000		0.464
Na	0.000	0.001	0.001	0.000	0.000		0.000	0.000	0.000		0.447
K	0.000	0.000	0.000	0.000	0.000		0.000	0.000	0.000		0.000
Mg#	88.9	81.4	77.6	89.4	84.9		75.3	77.9	78.4		
Activities[b]											
fo	0.79	0.66	0.60	0.80	0.72	sp	0.72	0.77	0.77	an	0.72
fa	0.012	0.035	0.050	0.011	0.023	herc	0.250	0.240	0.240	ab	0.56
						mt	0.0056	0.0001	0.0002		

[a] Calculated from stoichiometry

[b] As determined by Ax for THERMOCALC; See Holland and Powell (2003) for endmember abbreviations

Table 4 Trace-element mineral data (ICP-MS)

ppm	Garnet					Clinopyroxene							Detection limit
	06-07 Core	06-07 Rim	03-08 Core	03-08 Rim	± (1σ)	06-07 Core	06-07 Rim	03-08 Core	03-08 Rim	03-08 Cpx corona	03-08 Cpx corona	± (1σ)	
Rb	0.008	0.009	<0.038	<0.027	0.009	<0.006	0.005	<0.027	<0.033	0.341	1.720	0.009	0.006
Ba	<0.025	<0.020	<0.002	<0.068	0.019	0.064	0.130	<0.084	0.478	67.100	98.820	0.042	0.018
Th	<0.002	0.002	<0.017	<0.009	0.003	0.017	0.021	0.025	0.020	0.358	0.237	0.005	0.003
U	0.003	0.003	<0.010	<0.011	0.003	0.007	0.005	<0.009	<0.008	0.242	0.174	0.003	0.003
Nb	0.055	0.052	0.042	0.035	0.011	0.36	0.41	0.17	0.28	3.77	7.41	0.03	0.003
Ta	<0.002	<0.002	<0.011	<0.009	0.003	0.026	0.031	0.015	0.024	0.204	0.310	0.005	0.002
La	<0.003	0.005	<0.007	0.006	0.002	0.49	0.54	0.93	1.02	2.85	2.69	0.07	0.002
Ce	0.039	0.048	0.035	0.047	0.007	2.08	2.01	3.90	4.14	9.50	8.55	0.22	0.003
Pr	0.020	0.019	0.027	0.017	0.005	0.50	0.45	0.75	0.83	1.64	1.52	0.05	0.001
Sr	0.083	0.097	0.119	0.089	0.013	41.7	41.3	74.6	76.7	123.6	132.5	3.7	0.005
Nd	0.304	0.385	0.358	0.420	0.047	3.23	3.23	4.24	4.72	8.06	8.37	0.33	0.007
Sm	0.644	0.581	0.690	0.572	0.070	1.39	1.39	1.75	1.53	2.58	2.38	0.15	0.015
Zr	45.2	26.7	25.2	19.9	1.3	25.7	22.4	27.4	28.3	35.5	37.8	1.6	0.007
Hf	1.053	0.401	0.343	0.282	0.044	0.91	0.85	1.10	1.10	1.22	1.19	0.09	0.008
Eu	0.474	0.419	0.398	0.391	0.033	0.67	0.60	0.65	0.71	1.00	0.99	0.06	0.004
Gd	2.93	2.48	2.36	2.18	0.20	2.28	2.08	2.06	1.85	2.94	2.54	0.21	0.016
Tb	0.92	0.75	0.64	0.56	0.04	0.33	0.33	0.27	0.29	0.35	0.37	0.03	0.003
Dy	9.30	8.10	5.84	4.67	0.48	2.14	2.01	1.44	1.28	1.88	1.95	0.16	0.010
Y	68.9	61.6	39.4	31.5	2.7	8.93	9.14	4.45	4.87	7.01	6.73	0.48	0.003
Ho	2.61	2.23	1.43	1.14	0.11	0.35	0.34	0.18	0.21	0.30	0.29	0.02	0.003
Er	8.92	8.01	4.64	3.79	0.36	0.83	0.92	0.36	0.41	0.66	0.56	0.05	0.006
Tm	1.54	1.37	0.71	0.55	0.06	0.099	0.098	0.044	0.038	0.048	0.044	0.008	0.002
Yb	11.15	10.39	5.74	4.26	0.42	0.52	0.62	0.18	0.24	0.33	0.36	0.04	0.012
Lu	1.73	1.58	0.81	0.60	0.07	0.056	0.073	0.019	0.028	0.034	0.034	0.006	0.003

equilibration of the xenolith assemblage in the mantle and the development of decompression coronas at a depth of about 40 km below the surface, close to previous estimates of the base of the crust by Ionov (2002). The corona assemblages from sample 03-08 indicate temperatures that are about 200°C hotter than mantle conditions recorded by equilibrium between the primary compositions of the xenolith assemblage (and for lherzolite 06-08 the temperature increase may be even higher), a conclusion that is supported by the formation of reaction rims of olivine mantling orthopyroxene at the margin of the xenolith where pyroxene was in contact with the melt (Fig. 2d). This texture results from the incongruent melt reaction of orthopyroxene generating peritectic olivine. Heating is also indicated by the spongy reaction rim to clinopyroxene grains (Fig. 2e) suggesting loss of Na and Al to vermicular interstices which represent local melt pockets. These reaction textures do not distinguish between melt formation during decompression or during heating but the mineral thermometry (Fig. 5) clearly requires a strong heating input to the process.

The implied increase in temperature for the xenoliths suggests that melts were derived from mantle depths in excess of the depths at which the xenoliths were entrained (ca. 70 km). Independent evidence that the xenoliths were not cognate but entrained during magma ascent comes from the contrast in Sr–Nd–Pb isotope ratios between basalt and xenolith (Barry et al. 2003). This implies disequilibrium between melt and xenolith at the time of entrainment which is confirmed by considering the trace-element partitioning between garnet and clinopyroxenes and the host basalt. From published mineral/melt partition coefficients one can calculate the REE composition of the melt in equilibrium with the analysed mineral and compare these model melt compositions with the composition of the host basalt (Fig. 6). Mineral data from the Baga Togo Uul xenoliths show clear disequilibrium between the rim compositions of both garnet and clinopyroxene with melt. Both mineral compositions require a coexisting melt that is strongly depleted in LREE compared to the observed basaltic compositions from the region. These observations contrast with those from xenoliths of the Vitim volcanic

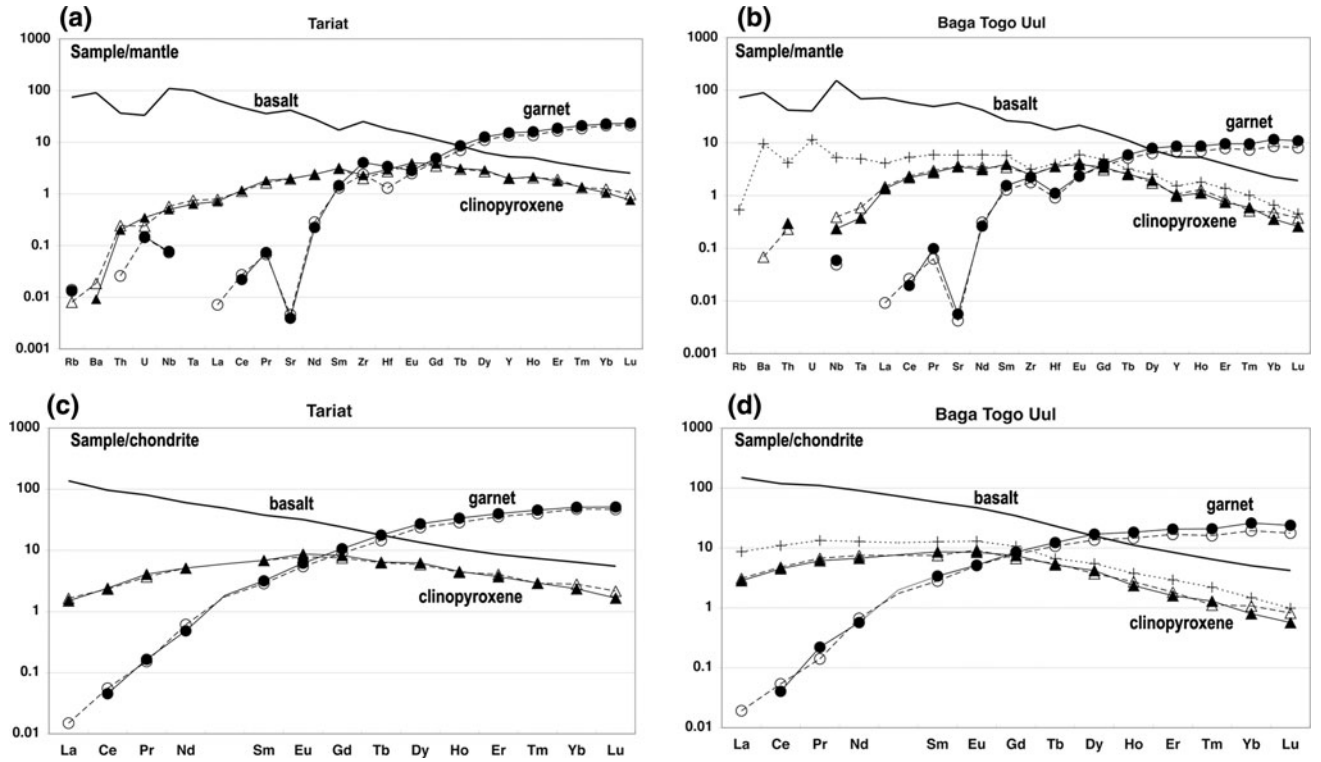

Fig. 4 ICP-MS trace-element data normalised against primitive mantle compositions (taken from Sun and McDonough 1989) for garnet and clinopyroxenes from **a** sample 06-07 (Tariat region); **b** sample 03-08 (Tulga vent, Baga Togo Uul). REE data, normalized against chondritic values (taken from Potts et al. 1981) for garnet and clinopyroxenes from **c** sample 06-07 (Tariat region); **d** sample 03-08 (Baga Togo Uul). Also plotted are analyses for basaltic compositions (heavy solid line); sample MN15.1.1 for Tariat plots (Mg# = 65, SiO_2 = 47%) and sample MN27.1 for Baga Togo Uul plots (Mg# = 68, SiO_2 = 45%), both from Barry et al. (2003). *Filled circle* garnet core (*solid line*), *open circle* garnet rim (*dashed line*), *filled triangle* clinopyroxene core (*solid line*), *open triangle* clinopyroxene rim (*dashed line*); *plus symbol* clinopyroxene in corona for Tulga sample (*dotted line*)

field (east of Baikal), where disequilibrium of garnet with melt is contrasted with clinopyroxene compositions that are close to equilibrium with the host alkali picrite (Glaser et al. 1999). In contrast to the primary phases, the clinopyroxene from the spongy corona enclosing primary clinopyroxene has clearly equilibrated with a melt of similar LREE composition to the host basalt. The HREE appear slightly depleted, but given that HREE in clinopyroxenes diffuse more rapidly than LREE (Van Orman et al. 2001), we infer that that this apparent depletion reflects uncertainties in the mineral/melt partition coefficients. Our data provide strong evidence that the clinopyroxene corona results from recrystallisation of the rim of a primary clinopyroxene grain in the presence of a basaltic melt (Fig. 2e). This pyroxene is strongly enriched in Rb, Ba, Th, U, Nb and Ta relative to pyroxenes in the same section that have equilibrated under garnet lherzolite conditions (Fig. 4b).

In theory, the timescale of xenolith entrainment and ascent can be constrained by considering the extent of chemical equilibration between xenolith minerals and melt. For garnet, diffusion rates of trivalent REEs are similar irrespective of their ionic radius but are two orders-of-magnitude slower than for divalent ions (Van Orman et al. 2002). For the garnet in the Baga Togo Uul sample, the rim analysis (Table 4) is 50 μm from the grain boundary; for this the timescales are 21 year for the equilibration of Ce and 25 years for Yb. Since the LREE in the garnet rim have clearly not equilibrated (Fig. 6), a first-order conclusion is that the xenolith has been entrained in the host melt for a period <21 years prior to crystallisation of the magma. A much tighter constraint for magmatic timescales can be obtained from the diffusion profile delineated by Mg# variations across an olivine traverse from sample 03-08 (Fig. 3). Equating the relationship $(Dt)^{0.5}$, where D = diffusion coefficient of Fe–Mg in olivine and t = time, to the half distance between core and rim compositions (21.75 μm) the diffusion profile of the Mg-depleted rim implies a timescale of about 4 days. These calculations assume a temperature of 1,200°C and use Fe–Mg diffusion rates from Jurewicz and Watson (1988) that were parameterised by Gaetani and Watson (2002) which are at an appropriate oxygen fugacity for the Mongolian xenoliths. A more rigorous approach using

Table 5 Outputs from thermobarometry for garnet-bearing mantle xenoliths

	Temperature (°C)				Pressure (Kbars)			
	P (kbars) (assumed)	*T*(1)	*T*(2)	THERMOCALC (Average T)	*T* (°C) (assumed)	*P*(1)	*P*(2)	THERMOCALC (Average T)
Tariat region								
06-07 (Shavaryn-Tsaram)	18	1,100	1,070		1,100	17.4	17.6	
18-07 (Shavaryn-Tsaram)	18	1,090	1,100		1,100	17.9	17.6	
ST-1 (Shavaryn-Tsaram)[a]	20	1,090	1,080		1,100	19.6	19.8	
Z68 (Zala)[a]	19	1,080	1,070		1,100	18.7	18.1	
Baga Togo Uul								
03-08 (Tulga; core assemblage)	20	1,000	965		1,000	22.0	19.3	
06-08 (Tulga; core assemblage)	20	1,000	995		1,000	22.1	19.3	
03-08 (Tulga; corona assemblage)	13	1,220	1,190	1,200 ± 180	1,200	12.7	14.7	13.1 ± 0.9
06-08 (Tulga; corona assemblage)	18	1,290	1,310	1,270 ± 140	1,300	17.2	19.9	

[a] Mineral compositions from Ionov et al. 1998

T(1) Brey and Köhler 1990; *T*(2) Nimis and Taylor 2000

P(1) Brey and Köhler 1990; *P*(2) Nimis and Taylor 2000

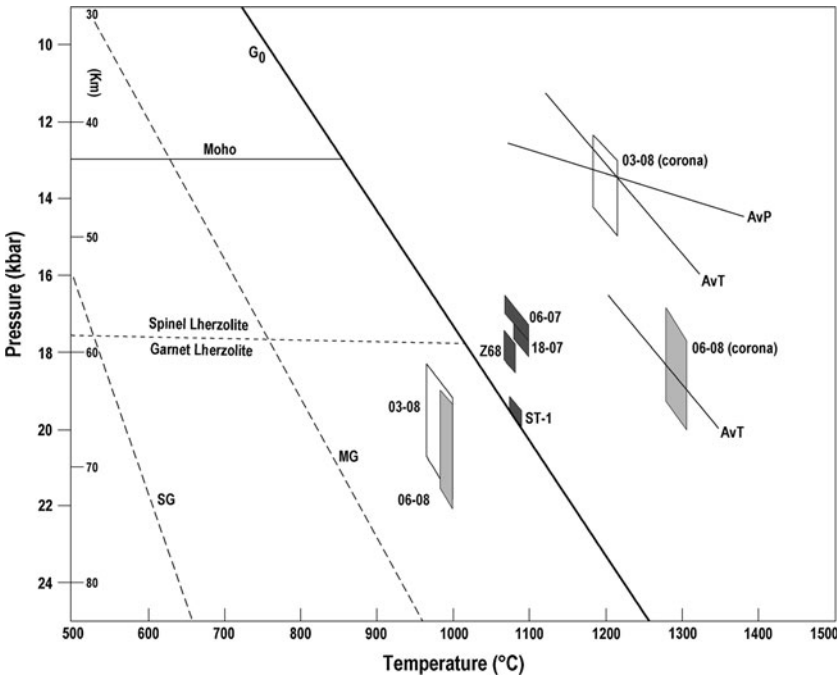

Fig. 5 Pressure–temperature plot for fields defined by outputs in Table 5. Estimates of crustal thickness and G_0, constrained by PT data from Tariat lherzolites and Pleistocene xenoliths from Vitim volcanics (Baikal), are from Ionov (2002). Boundary between spinel and garnet lherzolites defined by reaction (1) calculated from phases in lherzolite 06-08. Tariat data (dark grey fields) include garnet lherzolites (ST-1, Z68 from Ionov et al. 1998) and garnet websterite (06-07, 18-07 from Table 2). Data for garnet lherzolites from Tulga vent, Baga Togo Uul (white fields = 03-08, pale grey fields = 06-08) from Table 3. Size of *boxes* indicates range of results using thermobarometers listed in Table 5; uncertainties on individual thermometers are < ±30°C, and on barometers < ±2 kbars (Nimis and Taylor 2000). Average temperature (AvT) and average pressure (AvP) paths for corona assemblage derived from THERMOCALC; see text for details. *SG* geotherm for Siberian craton assuming heat flow 40 mW m^{-2} (Lysak and Dorofeeva 1997); *MG* geotherm for average Mongolian heat flow of 60 mW m^{-2} (Khutorskoy and Yarmoluk 1989)

regression analysis of the data and the semi-infinite media diffusion equation (see Parkinson et al. 2007) yields a more robust time span of 3.4 ± 0.8 days. This severely constrains any possible period of ponding at the Moho during ascent but rather suggests rapid ascent of basalt to the surface during which the garnets decompressed to

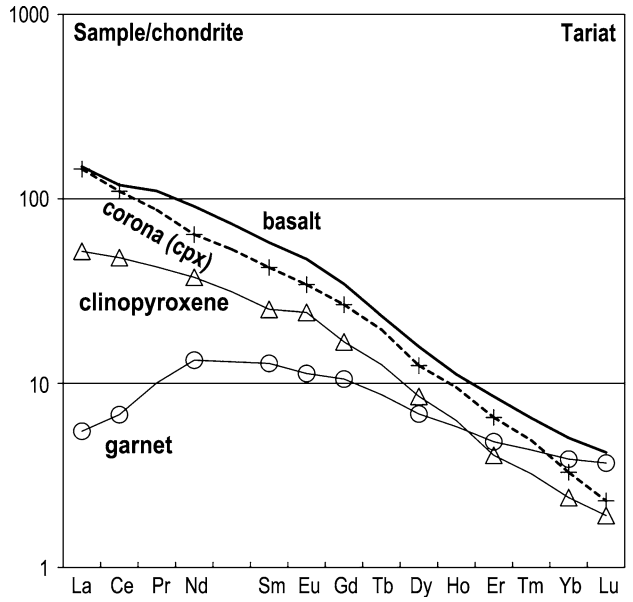

Fig. 6 Modelled REE abundances (chondrite normalized) for equilibrium melts calculated from trace-element abundances in garnet and clinopyroxene (Table 4, Fig. 4) from xenolith sample 03-08 (Tulga vent, Baga Togo Uul). Primary melt compositions for alkali basalt (heavy solid line) from sample MN27.1 (Barry et al. 2003). Modelling from compositions of garnet rim (*open circle*, *solid line*), clinopyroxene rim (*open triangle*, *solid line*) and from clinoproxene in corona for Tulga sample (*plus symbol*, *dotted line*). Assumed partition coefficients are from Hart and Dunn (1993) and Hauri et al. (1994)

develop corona assemblages. Given that the two samples with analysed corona structures (03-08, 06-08) record distinct pressures of equilibration (Fig. 5) it seems likely that the depths at which decompression textures developed were determined by reaction kinetics (locally modified by a_{H2O} in the melt) during a virtually continuous ascent. The implied average ascent rate of 0.2–0.3 m s^{-1} lies within the range of values (0.2–0.5 m s^{-1}) for the ascent of mafic alkali magma determined from FTIR analyses of olivine in peridotite xenoliths (Pesliera and Luhr 2006). The paucity of lherzolite xenoliths from the Baga Togo Uul region, may reflect their disaggregation during ascent (Brearley and Scarfe 1986). This speculation is supported by the high Ni and Cr abundances in some Togo basalts which may reflect disaggregated mantle xenoliths (Barry et al. 2003) and also by the occurrence of xenomorphic olivine with undulose extinction in host basalts.

Thermal constraints

Our work confirms previous studies of Tariat lherzolites, from the central region of the Hangay dome, in finding that the geotherm sampled by garnet-bearing xenoliths is indicative of high heat flow defining a lithospheric geotherm that is typical of intra-plate alkali basalt provinces (e.g. O'Reilly and Griffin 1985) requiring advective heating from mantle-generated basaltic melts (Cull et al. 1991). The elevated Tariat geotherm is also identical with that defined by xenoliths from Pleistocene volcanics of the Vitim field east of the Baikal rift (Ionov 2002). A high geotherm associated with the Baikal rift is also supported by the high potential mantle temperatures required to generate basaltic melts associated with the Vitim field (Johnson et al. 2005). The heat flow required to support this geotherm is 75–90 mW m^{-2} (Ionov 2002) compared with the average present-day value for Mongolia (60 mW m^{-2}; Khutorskoy and Yarmoluk 1989) and 40–50 mW m^{-2} for the Siberian platform (Lysak and Dorofeeva 1997). Our work demonstrates that, based on new mineral data from Pleistocene lherzolites at the north-east edge of the Hangay dome, this zone of anomalously high heat flow does not extend outside the margins of the dome over a distance of ca. 230 km (Fig. 1) although the geotherm for the periphery of the dome is still elevated above the average values for Mongolia (Fig. 5).

Recent teleseismic studies provide evidence for a thin lithosphere (<100 km) beneath the Hangay dome (Barruol et al. 2008). Given that the crust is above-average thickness (ca. 45 km) the sub-continental mantle lithosphere must be <55 km thick implying thermal erosion, possibly by a mantle plume. It is not possible that the Hangay thermal structure shares the same plume head as the Baikal rift since (1) teleseismic evidence suggests the diameter of the Baikal plume to be of the order of 100–200 km (Petit et al. 1998) whereas the Hangay dome lies 800 km south of the centre of the proposed Baikal plume and (2) the PT data from the garnet coronas from xenoliths on the margins of the dome (Tulga vent of Baga Togo Uul) suggest magmas of normal potential temperatures (ca. 1,300°C; McKenzie and Bickle 1988) restricting the dimensions of the Hangay anomaly to the region of topographic uplift measuring ca. 300 km across.

Conclusions

This study reports the first thermobarometric data from garnet-lherzolite xenoliths recovered from Pleistocene alkali basalt volcanoes near the rim of the Hangay dome (Togo region). Core analyses of coexisting pyroxenes and garnet indicate conditions of equilibration of $P = 18$–22 kbars and $T = 960$–1,000°C. Microtextures suggest the primary assemblages have been both heated, as evidenced by spongy olivine rimming orthopyroxene and by clinopyroxene being replaced by spongy low-Na, low-Al pyroxene overgrowths in chemical equilibrium with a basaltic melt, and decompressed, as evidenced by reaction coronas around garnet including spinel and/or plagioclase. Plagioclase-bearing coronas suggest equilibration at

$P = 12.5$–15.0 kbars, $T = 1{,}190$–$1{,}225$°C. Olivines are strongly zoned in such xenoliths and their diffusion profiles are indicative of periods of 3–4 days between entrainment of the xenolith and crystallisation at the surface. These data suggest the xenoliths have been decompressed through ~25 km to a depth of about 40–50 km where the decompression coronas developed before final ascent and extrusion. Corona assemblages indicate conditions about 200°C hotter than mantle conditions, suggesting melts were derived from mantle depths in excess of 70 km.

Garnet websterites and garnet lherzolites from volcanic centres at the centre of the Hangay dome (Tariat) indicate conditions of formation within the spinel lherzolite field ($P = 17$–18 kbars, $T \approx 1{,}090$°C) and garnet lherzolite field ($P = 18$–20 kbars, $T = 1{,}070$–$1{,}090$°C), respectively. These data indicate that a significantly steeper geotherm prevailed during magmatism at Tariat compared to the Togo region, the former being comparable with conditions derived from xenoliths associated with magmatism beneath the Baikal rift. Combined thermobarometric and geophysical data from the Hangay dome suggest that thermal anomalies in the mantle resulted in both its topographic uplift and in melting at the base of a thinned lithosphere.

Acknowledgments Fieldwork was supported by the Natural Environment Research Council (Alison Hunt) and the W G Fearnsides Fund administered by the Geological Society (Nigel Harris). We thank reviewers Dmitri Ionov and Bill Griffin for their insightful comments on the manuscript.

References

Agafonov LV, Pinus GV, Lesnov FP, Lavrent'ev YuG, Usova LS (1975) Abyssal inclusions in basaltoids from the Shavaryn-Saram pipe Mongolia. Doll Akad Nauk SSSR 225:1163–1165 (in Russian)

Badarch G, Cunningham WD, Windley BF (2002) A new terrane subdivision for Mongolia: implications for the Phanerozoic crustal growth of Central Asia. J Asian Earth Sci 21:87–110

Barruol G, Deschamps A, Déverchère J, Mordvinova VV, Ulziibat M, Perrot J, Artemiev AA, Dugarmaa T, Bokelmann GHR (2008) Upper mantle flow beneath and around the Hangay dome, Central Mongolia. Earth Planet Sci Lett 274:221–233

Barry TL, Saunders AD, Kempton PD, Windley BF, Pringle MS, Dorjnamjaa D, Saandar S (2003) Petrogenesis of Cenozoic basalts from Mongolia: evidence for the role of asthenospheric versus metasomatized lithospheric mantle sources. J Petrol 44:55–91

Brearley M, Scarfe CM (1986) Dissolution rates of upper mantle minerals in an alkali basalt melt at high pressure: an experimental study and implications for ultramafic xenolith survival. J Petrol 27:1157–1182

Brey GP, Köhler T (1990) Geothermobarometry in four-phase lherzolites 2. New thermobarometers and practical assessment of existing thermobarometers. J Petrol 31:1353–1378

Chuvashova IS, Rasskazov SV, Yasnygina TA (2007) Holocene volcanism in Central Mongolia and NE China: asynchronous decompressional and fluid melting of the mantle. J Volc Seismol 1:372–396

Cull JP, O'Reilly SY, Griffin WL (1991) Xenolith geotherms and crustal models in Eastern Australia. Tectonophysics 192:359–366

Cunningham WD (2001) Active intracontinental transpressional mountain building in the Mongolian Altai: defining a new class of orogen. Tectonophysics 331:389–411

Gaetani GA, Watson EB (2002) Modeling the major-element evolution of olivine-hosted melt inclusions. Chem Geol 183:25–41

Glaser SM, Foley SF, Günther D (1999) Trace element compositions of minerals in garnet and spinel peridotite xenoliths from the Vitim volcanic field, Transbaikalia, eastern Siberia. Lithos 48:263–285

Griffin WL, Powell WJ, Pearson NJ, O'Reilly SY (2008) GLITTER: data reduction software for laser ablation ICP-MS. In: Sylvester P (ed) Laser ablation-ICP-MS in the earth sciences. Mineral Assoc Canada Short Course Ser 40, Appendix 2, pp 204–207

Günther D, Heinrich CA (1999) Enhanced sensitivity in laser ablation-ICP mass spectrometry using helium-argon mixtures as aerosol carrier. J Anal At Spectrom 14:1363–1368

Harris N (2009) Of all places, why here? Geoscientist 19:21–23

Hart SR, Dunn T (1993) Experimental clionopyroxene/melt partitioning of 24 trace elements. Contrib Mineral Petrol 113:1–8

Hauri EH, Wagner TP, Grove TL (1994) Experimental and natural partitioning of Th, U, Pb and other trace elements between garnet, clinopyroxene and basaltic melts. Chem Geol 117:149–166

Holland TJB, Powell R (1998) An internally consistent dataset for phases of petrological interest. J Metamorphic Geol 16:309–343

Holland TJB, Powell R (2003) Activity–composition relations for phases in petrological calculations: an asymmetric multicomponent formulation. Contrib Mineral Petrol 145:492–501

Hunt AC, Parkinson IJ, Rogers N, Harris N, Barry T, Uondon M (2008) Deciphering the sources and melt generation mechanisms of Cenozoic intraplate volcanism in central Mongolia. Geochim Cosmochim Acta 72:A403 (abstract)

Ionov D (2002) Mantle structure and rifting processes in the Baikal–Mongolia region: geophysical data and evidence from xenoliths in volcanic rocks. Tectonophysics 351:41–60

Ionov DA (2007) Compositional variations and heterogeneity in fertile lithospheric mantle: peridotite xenoliths in basalts from Tariat, Mongolia. Contrib Mineral Petrol 154:455–477

Ionov DA, Hoefs J, Wedepohl KH, Wiechert U (1992) Content and isotopic composition of sulphur in ultramafic xenoliths from central Asia. Earth Planet Sci Lett 111:269–286

Ionov DA, O'Reilly SY, Griffin WL (1998) A geotherm and lithospheric cross-section for central Mongolia. In: Flower MJF, Chung S-L, Lo C-H, Lee TY (eds) Mantle dynamics and plate interactions in East Asia. Amer Geophys Union Geodynamics Ser 27, Washington, DC, pp 127–153

Johnson JS, Gibson SA, Thompson RN, Nowell GM (2005) Volcanism in the victim volcanic field, Siberia: geochemical evidence for a mantle plume beneath the Baikal rift zone. J Petrol 46:1309–1344

Jurewicz AJG, Watson EB (1988) Cations in olivine, Part 2. Diffusion in olivine xenocrysts, with applications to petrology and mineral physics. Contrib Mineral Petrol 99:186–201

Khutorskoy MD, Yarmoluk VV (1989) Heat flow, structure and evolution of the lithosphere of Mongolia. Tectonophysics 164:315–322

Kopylova MG, O'Reilly SY, Genshaft YS (1995) Thermal state of the lithosphere beneath Central Mongolia: evidence from deep-seated xenoliths from the Shavaryn-Saram volcanic centre in the Tariat depression, Hangay, Mongolia. Lithos 36:243–255

Lysak SV, Dorofeeva RP (1997) Geothermal regime of the upper horizons of the earth's crust in the southern regions of Eastern Siberia. Trans Dokl Russ Acad Sci Earth Sci Sect 352:133–137

McKenzie D, Bickle MJ (1988) The volume and composition of melt generated by extension of the lithosphere. J Petrol 29:625–679

Nickel KG, Green DH (1985) Empirical geothermobarometry for garnet peridotites and implications for the nature of the lithosphere, kimberlites and diamonds. Earth Planet Sci Lett 73:158–170

Nimis P, Taylor WR (2000) Single clinopyroxene thermobarometry for garnet peridotites. Part I. Calibration and testing of a Cr-in-Cpx barometer and an enstatite-in-Cpx thermometer. Contrib Mineral Petrol 139:541–554

O'Reilly SY, Griffin WL (1985) A xenolith-derived geotherm for southeastern Australia and its geophysical implications. Tectonophysics 111:41–63

Parkinson IJ, Hammond SJ, James RH, Rogers NW (2007) High-temperature lithium isotope fractionation: Insights from lithium isotope diffusion in magmatic systems. Earth Planet Sci Lett 257:609–621

Pesliera AH, Luhr JF (2006) Hydrogen loss from olivines in mantle xenoliths from Simcoe (USA) and Mexico: Mafic alkalic magma ascent rates and water budget of the sub-continental lithosphere. Earth Planet Sci Lett 242:302–319

Petit C, Koulakov I, Deverchère J (1998) Velocity structure around the Baikal rift zone from teleseismic and local earthquake travel times and geodynamic implications. Tectonophysics 296:125–144

Potts PJ, Thorpe OW, Watson JS (1981) Determination of the rare-earth element abundances in 29 international rock standards by instrumental neutron activation analysis: A critical appraisal of calibration errors. Chem Geol 34:331–352

Pouchou JL, Pichoir F (1985) "PAP" procedure for improved quantitative analysis. Microbeam Anal 20:104–105

Press SG, Witt HA, Seck DA, Ionov DA, Kovalenko VI (1986) Spinel peridotite xenoliths from the Tariat depression, Mongolia. 1: Major element chemistry and mineralogy of a primitive mantle xenolith suite. Geochim Cosmochim Acta 50:2587–2599

Schlupp A (1996) Néotectonique de la Mongolie occidentale analysée à partir de données de terrain, sismologiques et satellitaires. PhD thesis, Université Louis Pasteur de Strasbourg

Sobolev NV, Nixon PH (1987) Xenoliths from the USSR and Mongolia: a selective and brief review. In: Nixon PH (ed) Mantle xenoliths. Wiley, New York, pp 159–166

Stosch HG, Ionov DA, Puchtel IS, Galer SJG, Sharpouri A (1995) Lower crustal xenoliths from Mongolia and their bearing on the nature of the deep crust beneath central Asia. Lithos 36:227–242

Sun SS, McDonough WF (1989) Chemical and isotopic systematics of oceanic basalts: implications for mantle composition and processes. In: Saunders AD, Norry MJ (eds) Magmatism in the Ocean Basins. Special Publications, Geological Society of London 42, pp 313–345

Van Orman JA, Grove TL, Shimizu N (2001) Rare earth element diffusion in diopside: influence of temperature, pressure and ionic radius, and an elastic model for diffusion in silicates. Contrib Mineral Petrol 141:687–703

Van Orman JA, Grove TL, Shimizu N, Layne GD (2002) Rare earth element diffusion in a natural pyrope single crystal at 2.8 GPa. Contrib Mineral Petrol 142:416–424

Walker RT, Molor E, Fox M, Bayasgalan A (2008) Active tectonics of an apparently aseismic region: distributed active strike-slip faulting in the Hangay Mountains of central Mongolia. Geophys J Int 174:1121–1137

Wells PRA (1977) Pyroxene thermometry in simple and complex systems. Contrib Mineral Petrol 62:129–139

Williams HM, Turner SP, Pearce JA, Kelley SP, Harris NBW (2004) Nature of the source regions for post-collisional, potassic magmatism in Southern and Northern Tibet from geochemical variations and inverse trace element modelling. J Petrol 45:555–607

Windley BF, Allen MB (1993) Mongolian plateau: evidence for a late Cenozoic mantle plume under central Asia. Geol 21:295–298

Windley BF, Alexeiev D, Xiao W, Kröner A, Badarch G (2007) Tectonic models for accretion of the Central Asian Orogenic Belt. J Geol Soc 164:31–47